Comprehensive Study of Carrier Recombination in High-Efficiency CdTe Solar Cells Using Transient Photovoltage

Abasi Abudulimu, Steven Carter, Adam B. Phillips, Deng-Bing Li, Sabin Neupane, Tyler Brau, Jared Friedl, Ebin Bastola, Manoj K. Jamarkattel, Michael J. Heben, Yanfa Yan, and Randy J. Ellingson**

Cadmium telluride (CdTe) solar cells represent a commercially successful photovoltaic technology, with an annual production capacity approaching 20 GW. However, improving the open-circuit voltage (V_{OC}) remains challenging. This study aims to deepen the understanding of charge carrier recombination in CdTe solar cells and to explore alternative dynamical characterization methods that address the limitations found in conventionally used time-resolved photoluminescence for CdTe solar cells. Transient photovoltage and transient photocurrent techniques are utilized to investigate charge carrier dynamics under conditions resembling real-world solar cell operation. The results reveal that an effective nonradiative recombination lifetime of 580 ns dominates the charge dynamics at V_{OC} values below 850 mV. Above this threshold, radiative recombination becomes significant, with a radiative recombination coefficient of 1.1×10^{-9} cm^3 s^{-1}. Additionally, the stationary charge carrier density at 1 sun is determined to be around 1×10^{14} cm^{-3}. By accurately determining both radiative and nonradiative recombination, this work provides a comprehensive understanding of carrier dynamics in high-performing CdTe devices and paves the way for improving the V_{OC} and performance of CdTe solar cells.

1. Introduction

Cadmium telluride (CdTe) solar cells are at the leading edge of photovoltaic technology, with current module efficiencies surpassing 19% and small-area cell efficiencies reaching 22.3%.[1,2] However, realizing high open-circuit voltage (V_{OC}) remains a considerable challenge.[3–7] Efficient power conversion in solar cells depends on the generation, transport, and collection of charge carriers, processes which are sensitive to the absorber layer's characteristics and to the device interfaces.[8–18] Charge carrier dynamics within this framework are described by the drift-diffusion equation,[19] which for electrons in one dimension is:

$$\frac{\partial n(x,t)}{\partial t} = D\frac{\partial^2 n(x,t)}{\partial x^2} + \mu E\frac{\partial n(x,t)}{\partial t} + G(x,t) - R(n(x,t)) \tag{1}$$

This equation accounts for electron concentration $n(x,t)$, diffusion coefficient D, electron mobility μ, electric field E, generation rate $G(x,t)$, and recombination rate $R(n(x,t))$, which includes radiative and nonradiative (in the bulk and surfaces) recombination contributions. A similar equation can be applied for holes.

Device performance is typically characterized under illuminated steady-state conditions, where generation rate (G) equals the sum of recombination (R) and extraction (E_{xt}) rates, using voltage sweeps to measure current density. Under such conditions, the steady-state current density (J_{ext}) is proportional to the extraction rate and can be expressed as a function of generation and recombination rates.[20]

$$J_{ext}(V) = edE_{xt} = ed(G - R) \tag{2}$$

where e is the electric charge and d is the absorber thickness. Equation (2) shows that performance at steady state is determined by the interplay of carrier extraction (measured current density) and recombination. At V_{OC}, where no extraction occurs, the generation rate equals the recombination rates, which, when the radiative and nonradiative terms are explicitly considered, leads to:

$$G = R = n\left(\frac{1}{\tau_{rad}} + \frac{1}{\tau_{srh}}\right) = \frac{n}{\tau_{eff}}, \qquad \tau_{rad} = \frac{1}{kn} \tag{3}$$

A. Abudulimu, S. Carter, A. B. Phillips, D.-B. Li, S. Neupane, T. Brau, J. Friedl, E. Bastola, M. K. Jamarkattel, M. J. Heben, Y. Yan, R. J. Ellingson
Department of Physics and Astronomy and Wright Center for Photovoltaics Innovation and Commercialization
The University of Toledo
2600 Dorr Street, Toledo, OH 43606, USA
E-mail: abasi.abudulimu@utoledo.edu; randy.ellingson@utoledo.edu

The ORCID identification number(s) for the author(s) of this article can be found under https://doi.org/10.1002/solr.202400131.

DOI: 10.1002/solr.202400131

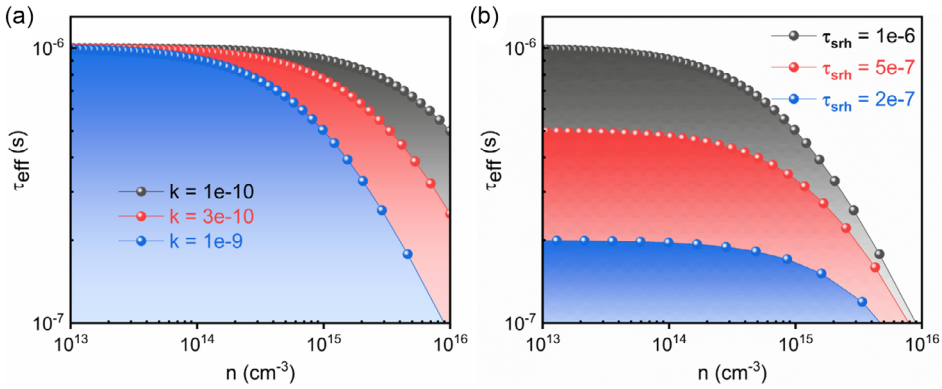

Figure 1. Illustration of the effective carrier lifetime dependence on the carrier concentration: for different a) radiative recombination coefficients and b) nonradiative recombination lifetimes.

In this scenario, τ_{rad}, τ_{srh}, and τ_{eff} represent the radiative, nonradiative, and effective carrier lifetimes, and k denotes the radiative recombination coefficient. Equation (3) shows that the shortest lifetime at any given carrier concentration dominates the recombination. **Figure 1** illustrates how the effective carrier lifetime τ_{eff} varies with carrier concentration n. At low n, τ_{rad} is long as it is inversely proportional to n; thus, the nonradiative recombination τ_{srh} dominates in this region, which is governed by defect density, capture rate, and surface recombination velocity.[21–23] At high n, radiative recombination dominates and follows the functionality defined in Equation (3). This behavior underscores the importance of measuring and presenting carrier lifetimes as a function of carrier density to fully understand the influence of different recombination mechanisms at distinct operational states of the solar cell. While radiative recombination is dictated by the radiative recombination coefficient k, an intrinsic property of the material, the nonradiative recombination can be avoided by passivating defects in the bulk and surface. Therefore, mitigating non-radiative recombination and precisely measuring τ_{nr} is vital for understanding how to approach the radiative limit of V_{OC}.

In CdTe devices, these lifetimes are typically probed using time-resolved photoluminescence (TRPL) measurements.[3,4,24] However, the measurements often being conducted on partial or fully completed devices in the CdTe community, interpretation of the TRPL data is difficult because in addition to the recombination, the electric field and carrier concentrations in the device also change with time.[25–27] Transient photovoltage (TPV) and current (TPC) measurements offer an alternative method in which the device is held under steady-state bias-light illumination and probed using a small perturbative laser pulse that does not result in changes to the electric field or carrier concentration.[28] Both TPV and TPC have been applied to a variety of photovoltaic materials but not yet to CdTe devices.[20,29–33] Here we use TPV and TPC to investigate a CdTe device. Since these techniques are new to the CdTe community, we start by comparing TRPL to TPV and TPC measurements. We then investigate a 19.2% efficient selenized CdTe absorber-based device.[4,6,34] We show that performing TPV and TPC measurements under different bias-light intensities allows to determine the stationary charge carrier density and the corresponding carrier lifetimes, producing the shape predicted by Equation (3). The nonradiative recombination with a lifetime of 580 ns dominates recombination at charge density below $1 \times 10^{14}\,cm^{-3}$, and above that, the radiative recombination starts to act with a radiative recombination coefficient of $1.1 \times 10^{-9}\,cm^{-3}\,s^{-1}$.

2. Challenges in Utilizing Time-Resolved Photoluminescence for Carrier Recombination Analysis in CdTe Solar Cells

TRPL serves as a pivotal, noninvasive technique for probing charge carrier dynamics in semiconductor devices.[28,35] This method involves photoinducing a transient excited state in a sample by a short laser pulse with small spot size (**Figure 2**a) and monitoring the subsequent photoluminescence decay to infer carrier recombination processes (Figure 2b). The decay curves obtained are typically analyzed using curve-fitting techniques that employ exponential functions to extract carrier lifetimes. However, TRPL decay is an outcome of continuously evolving multiple complex processes that take place in the sample.[27,28,36] Figure 2d depicts a simplified illustration of the complex processes represented by the evolution of quasi-Fermi-level splitting (QFLS) in time and 1D space. Prior to photoexcitation ($t = 0$ ps), the QFLS is 0 as the sample is in the dark equilibrium. Upon photoexcitation ($t = 1$ ps), the QFLS is enormous at the illumination side of the absorber, and it is small at the back. During and after photoexcitation, carrier extraction to electron transporting layer (ETL) and carrier diffusion to the back of the sample take place. While the QFLS in the absorber quickly reaches an equilibrium (within few hundreds of ps) due to the fast carrier diffusion in CdTe, illustrated as QFLS at $t = 1$ ns, it can take tens (even hundred depending on the properties of charge transporting layers) of nanoseconds to reach equilibrium throughout the device and build up voltage potentials between the two electrodes equal to that in the absorber. After this stage, $t \geq 100$ ns, the QFLS decays in time primarily due to carrier recombination (radiative and nonradiative), as depicted in Figure 2c. Note though that the carrier recombination is present during the whole process starting already from the carrier generation stage. It is worth mentioning that, in an ideal case where a TRPL setup

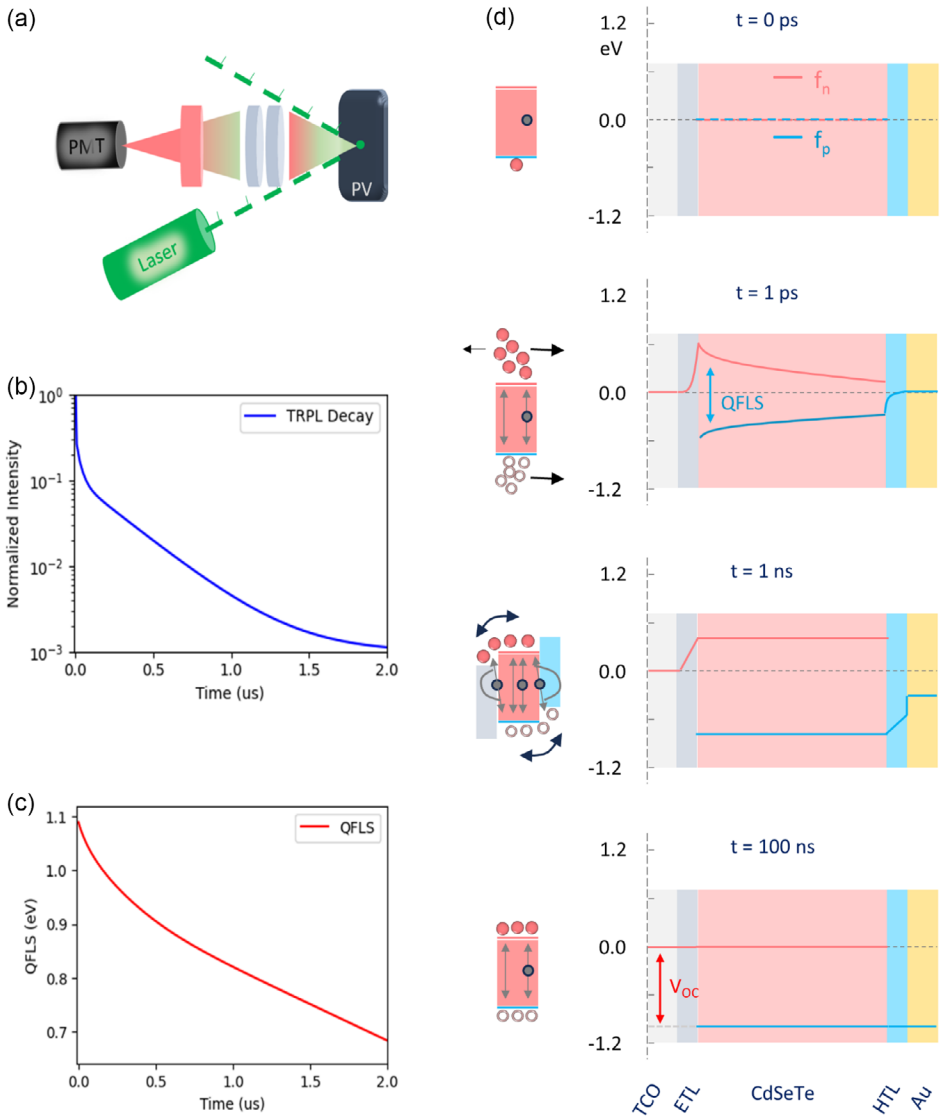

Figure 2. Illustration of TRPL: a) measurement principle; b) exemplary data, within which evolving carrier concentration and QFLS via drift, diffusion, and recombination are embedded; c) evolution of QFLS solely from recombination; and d) evolution of the QFLS throughout the device before and after photoexcitation.

is able to detect five or even higher orders of magnitude change in signal at a much lower repetition rate (<100 KHz), TRPL decay can also be influenced by the reinjection of the carriers, from electrodes to absorber, and by the detrapping of the carriers from shallow defects.[25,27,28,37]

All those information is embedded in a single TRPL decay data, and deciphering it and extracting accurate carrier lifetimes become difficult for CdTe samples with graded absorber and other layers.[25] The multiexponential decay form often observed in measurements of CdTe film stacks highlights the complexity of the TRPL data, and it is common in the CdTe community to assign τ_1 to the interface or surface recombination and τ_2 to bulk recombination. While multiexponential fitting indeed sheds light on the existence of different recombination processes, it is only valid when the redistribution of charge carrier density in the sample is minimal, and charge extraction is negligible. Otherwise, it falls short of providing a precise attribution of these processes to specific physical mechanisms within the cell. Accurate analysis of the TRPL data thus extends beyond simple decay models, additionally requiring comprehensive numerical simulations which incorporate the full scope of drift-diffusion equations to consider spatially and temporally variant carrier transport.[25,27,36] Most of the issues can be avoided if the measurement is done on the absorber deposited on a glass (or any substrate that does not interact with the absorber), as in such structures, the complex charge dynamics arising from the interplay of carrier diffusion, electric field-induced drift, and extraction can be eliminated. However, due to the concerns of different film growth on different substrates, conducting TRPL measurements on partial or fully completed device stack is common practice in CdTe community.

3. Transient Photovoltage and Photocurrent Techniques

TPV and TPC have been used as essential methodologies for probing carrier dynamics in various solar cell technologies.[29–33,38] Conducted under steady-state illumination conditions that closely resemble real-world operation, TPV measures changes in V_{OC} in response to a small perturbation in carrier concentration. The principle of the technique is illustrated in **Figure 3**a,b. The measurement starts with holding the device at a constant V_{OC} via a bias-light continuously illuminating throughout the measurement. Then, a brief weak laser pulse will be applied on top of the steady-state illumination, introducing a perturbing voltage (ΔV_{OC}) that decays over time. Ideally, the decay rate of the perturbed ΔV_{OC}, proportional to the rate of change of the perturbed charge carriers (Δn), is characterized by an effective carrier lifetime (τ_{eff}), as described by the equation.[29]

$$\frac{d\Delta V_{OC}}{dt} \propto \frac{d\Delta n}{dt} = -\frac{\Delta n}{\tau_{eff}} \tag{4}$$

Yet, in practice, the lifetime of a TPV decay, τ_{TPV}, can be influenced by the device capacitance C.[30,31,39–41] In this manuscript, we adhere to the simplified form proposed by Kiermasch et al.[40] where the measured TPV lifetime is expressed as the sum of

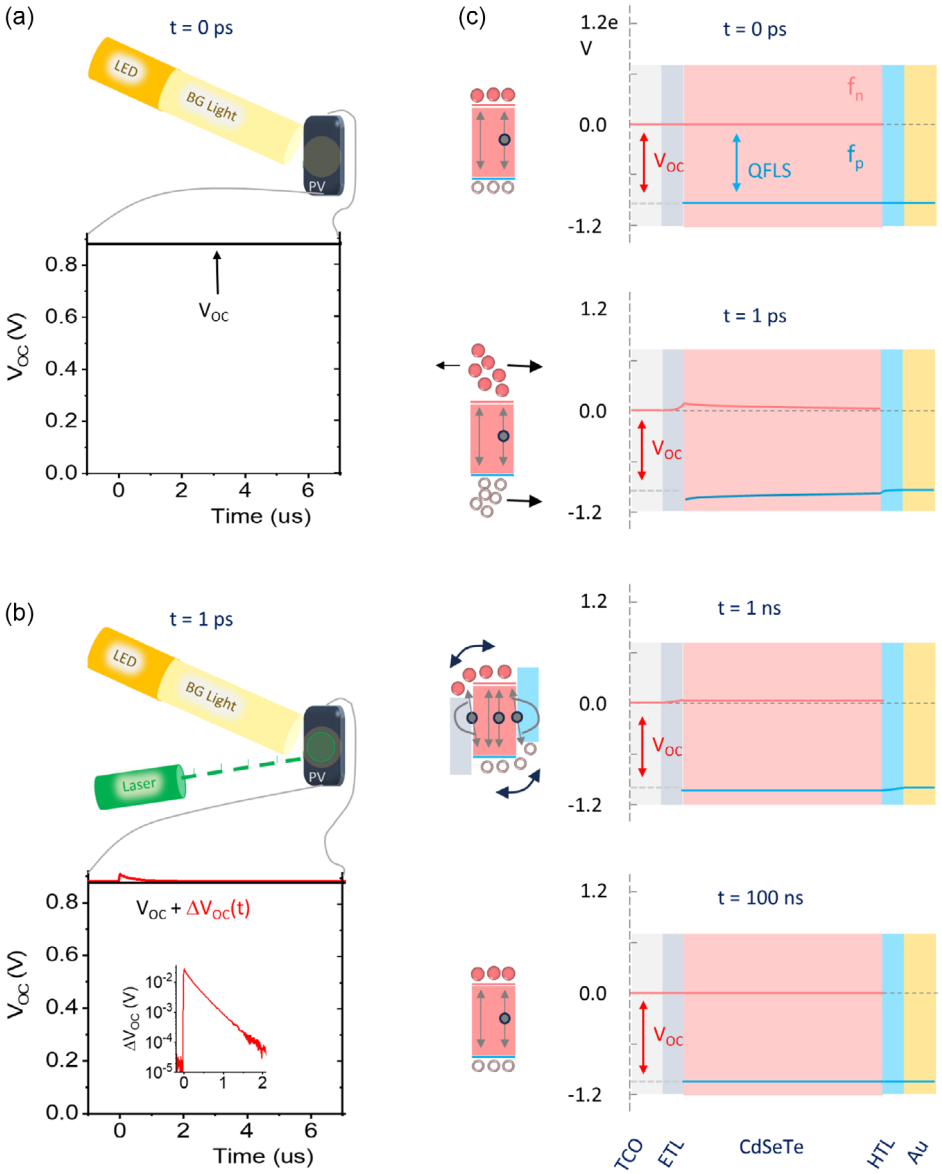

Figure 3. Illustration of the TPV Technique: a) Initially, the device is maintained under continuous bias-light illumination, resulting in a constant V_{OC}; b) a weak pulsed laser, superimposed on the bias-light intensity, induces a perturbation voltage $\Delta V_{OC}(t)$, which decays over time as depicted in the subfigure; c) similar to TRPL, this illustrates the QFLS evolution within the device before and after photoexcitation, characterized by the drift, diffusion, and recombination of carrier concentration.

capacitance decay constant τ_c and the effective lifetime of the photogenerated carriers.

$$\tau_{TPV} = \tau_c + \tau_{eff}, \qquad \tau_c = C\,R_{diode} \tag{5}$$

The derivation (see supporting document) of Equation (5) is rooted in the analytical solutions for a charge control model that describes the electrical behavior of solar cells with capacitance contributions, provided by Castaner et al.[42] and applied in the works of Kiermasch et al.[40] Sandberg et al.[31] provided a more complete form of it by incorporating external resistances such as R_{sh} and R_{load}. However, the impact of external resistance on our TPV data, measured with bias-light intensity >0.005 sun, is negligible. Equation (5) has reproduced the experimental data of organic and perovskite solar cells,[31,40] as well as our CdTe solar cells, well. However, we acknowledge the potential complexities and the evolving nature of this field, and the model should be revisited and refined as more data becomes available.

τ_c is the product of capacitance and diode resistance. R_{diode} can be obtained from a dark J–V or approximated from a light intensity-dependent $J_{SC}(V_{OC})$ measurement.

$$R_{diode} = \frac{n_{id}k_B T}{qJ_0}\exp\left(-\frac{qV_{OC}(t)}{n_{id}k_B T}\right) \approx \frac{n_{id}k_B T}{qJ_{SC}(V_{OC})} \tag{6}$$

where k_B is the Boltzmann constant, T is the temperature, n_{id} is the diode ideality factor, and J_{SC} (V_{OC}) is the current density corresponding to the V_{OC} measured at each bias-light intensity. Given that all the necessary parameters for determining the capacitive contribution to the TPV decay are readily accessible from the TPV and TPC data, one can account for the capacitive contribution τ_c and focus on understanding τ_{eff}.

TPV distinguishes itself from TRPL in several key aspects. As illustrated in Figure 3c, the charge distribution and the QFLS are uniform across the device due to the continuous bias-light illumination, and the impact of the perturbation pulse on that equilibrium condition is minimal, meaning that the effects of drift and diffusion on the TPV signal can be negligible. These factors lead to the simplification of Equation (1) to a recombination only Equation (7), allowing a more straightforward interpretation of the recombination dynamics in CdTe-based solar cells:

$$\frac{\partial n(t)}{\partial t} \approx G - R(n) \approx -\Delta n(t)/\tau_{eff} \tag{7}$$

Here, G is generation rate defined by the steady-state bias-light, $n(t)$ represents the carrier concentration at time t, comprising a steady-state concentration (n_{bias}) and a transient component ($\Delta n(t)$), with n_{bias} being much larger than Δn. The effective lifetime τ_{eff} is a composite of the radiative τ_{rad} and nonradiative τ_{srh} recombination lifetimes:

$$\tau_{eff} = \left[\frac{1}{\tau_{rad}} + \frac{1}{\tau_{srh}}\right]^{-1}, \qquad \tau_{rad} = \frac{1}{2kn_{bias}} \tag{8}$$

Here, k is the radiative recombination coefficient. Equation (8) differs from Equation (3) only on the radiative recombination component by a factor of ½. It is worth mentioning that in a TRPL decay, the carrier concentration, and so the QFLS, continuously changes after the generation, but, in a TPV measurement, they are fixed by the bias-light intensity. Thus, it is important to conduct TPV measurements across various bias-light intensities to fully understand the influence of different recombination mechanisms at different carrier concentrations. It should be noted that while τ_{srh} is a constant (as soon as the defects are not dynamics), τ_{rad} is a function of carrier density, as Equation (8) states.

The stationary carrier concentration n_{bias} at each bias-light intensity is achievable by combining TPV with TPC measurements, performed under the same bias-light conditions, as illustrated in **Figure 4**. TPC measures the change in current collection due to the perturbative pulse. Experimentally, TPC measurements are performed the same as TPV except the device output is connected to the 50 Ω oscilloscope input (approximating a short-circuit condition), as opposed to the 1 MΩ channel used in TPV (approximating an open-circuit condition), to allow current to flow.[20,29,32] The integration of the TPC decay curve (laser perturbation induced short-circuit current density change $\Delta J_{SC}(t)$) ΔQ, when normalized by the amplitude of the perturbation-induced voltage change ($\Delta V_{OC}(t=0)$), yields the differential capacitance, $C(V_{OC}) = \Delta Q/\Delta V_{OC}$, as illustrated in Figure 4. This data, when processed across different V_{OC} or bias-light intensities, enables the determination of stationary carrier density via Equation (9).[29]

$$n_{bias}(V_{OC}) = \frac{1}{Aed}\int_0^{V_{oc}} C\,dV = n_0 e^{\gamma V_{OC}} \tag{9}$$

where γ is a constant. Thus, the combined application of TPV and TPC techniques under a range of bias-light intensities allows for the quantification of stationary carrier densities under varying solar cell operational conditions and enables distinguishing the contributions of nonradiative and radiative recombination to overall device performance.

4. Experimental Transient Photovoltage and Photocurrent Data Measured on a High-Performance CdTe Device

Here we present the experimental results from TPV and TPC measurements conducted on a CdTe device that has resulted in a power conversion efficiency of 19.2% under one-sun AM1.5G illumination (other relevant data can be found in the supporting document). More information about the device performance and fabrication procedures can be found in our previous publication.[4,6,34] The device schematics and the current–voltage characteristics under one sun illumination are given in **Figure 5**. TPV measurements, **Figure 6**a, show that an increase in bias-light intensity leads to a concurrent rise in the stationary open-circuit voltage V_{OC} and an accelerated decay of ΔV_{OC} (Figure 6b). The former is due to the rise of the QFLS following the increase of the stationary carrier density n_{bias} with the bias-light intensity. The latter is because of the decrease of the diode resistance (coupled into τ_c in Equation (5))[31,40,41] and the reduction in effective carrier lifetime (τ_{eff} in Equation (5)) with the increase of radiative recombination rate. The formation of straight lines on the log–linear plot (Figure 6b), a single-exponential decay model, suggests that the decay of ΔV_{OC} is governed by a single dominant

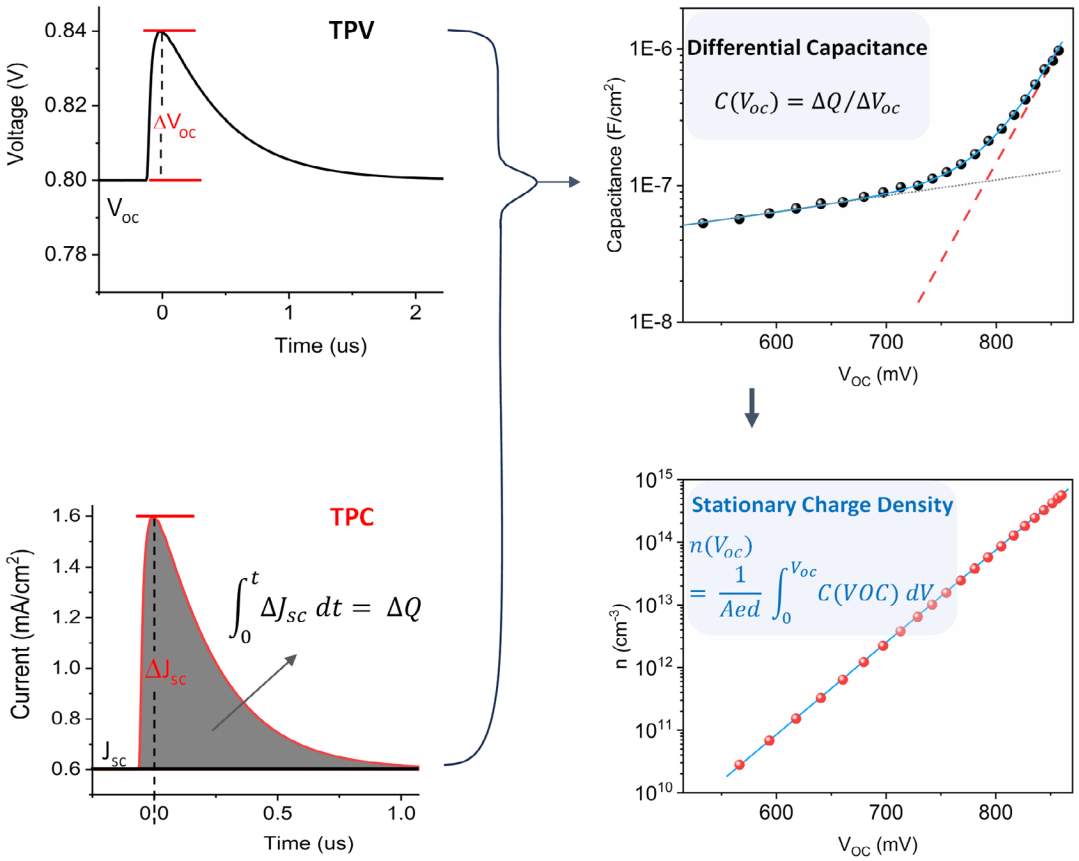

Figure 4. Illustration of obtaining differential capacitance C and stationary carrier density n_{bias} from TPV and TPC dataset measured at various bias-light intensities. In the capacitance graph (upper right), the gray dotted line indicates the depletion layer capacitance,[31,33] the red dashed line indicates the chemical capacitance induced by the photogeneration of the charge carriers in the absorber, and the blue solid line is the sum of those two. The stationary carrier density n_{bias} (the lower right graph) is derived by integrating the chemical capacitance over the V_{OC} values measured under different bias-light intensities and normalizing the area of device's active layer and the thickness. It grows exponentially with the V_{OC}, as Equation (9) states.

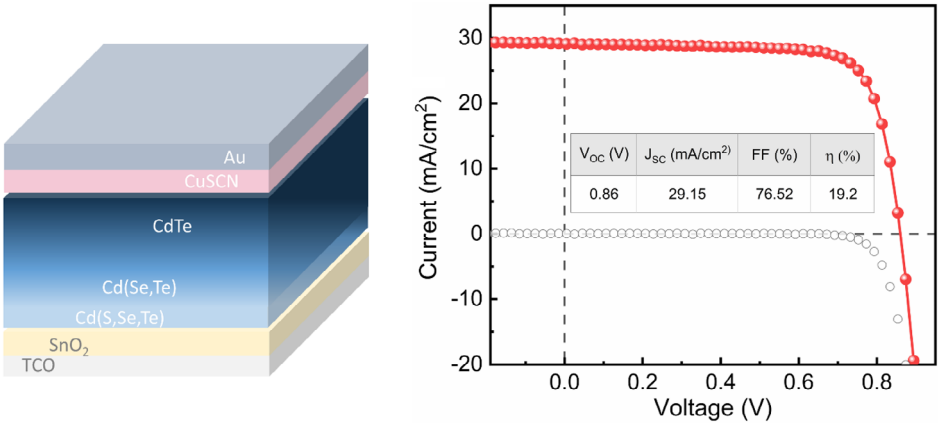

Figure 5. Schematics of the CdTe device and the J–V performance under 1 sun AM1.5G illumination.

mechanism in the device set by the bias-light intensity, and the influence of the perturbation is minimal, aligning well with the theoretical discussion detailed around Figure 3.

A deeper analysis, as presented in Figure 6c, focuses on the TPV lifetime τ_{TPV}, derived from the single-exponential fit of the ΔV_{OC} decay data. Note that we plotted τ_{TPV} against the V_{OC} (corresponding to the applied bias-light intensity) instead of carrier density, because V_{OC} is a measured parameter directly accessible from the TPV data and logarithmically dependent on the carrier density (see Equation (9)), whereas extracting the carrier density

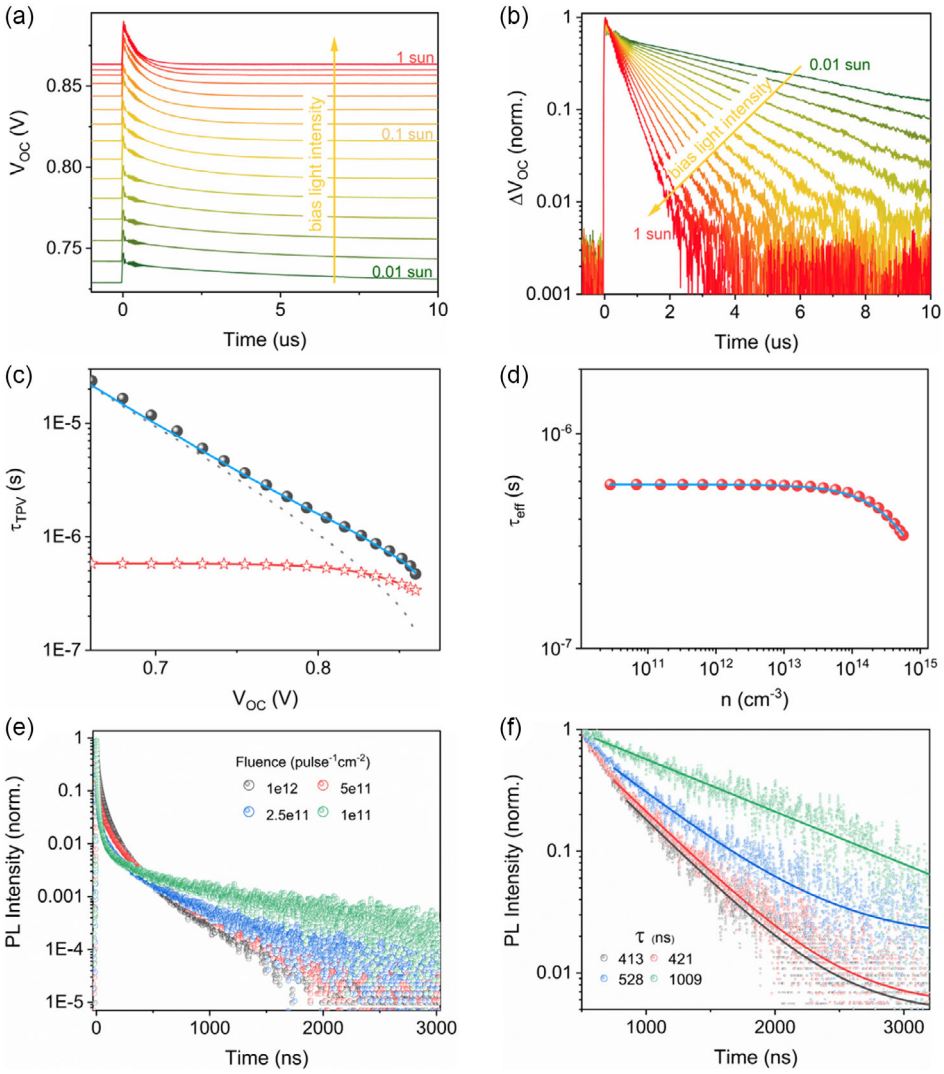

Figure 6. a) TPV measurement data at various bias-light intensities; b) only the time-dependent part of the TPV signal $\Delta V_{OC}(t)$ (the bias-light-induced constant V_{OC} is subtracted); c) TPV lifetime, dark circle symbols, extracted via single-exponential decay fit to the data in (b), where the gray dotted line is the capacitive contribution τ_c, the red star symbols are effective carrier recombination lifetime τ_{eff}, and the solid blue line is the sum of the two, based on Equation (5); d) effective carrier lifetime τ_{eff} as a function of stationary carrier density n_{bias} (acquired as illustrated in Figure 4), the solid blue line is a fit based on Equation (8). e) TRPL data measured at four different laser fluences, and f) the same data normalized at $t = 500$ ns. The solid lines represent single-exponential decay fits, and the resulting lifetimes are given in the inset.

from TPV and TPC requires further processing the data as explained in Figure 4. Also, it cannot be determined from the bias-light intensity without knowing τ_{srh} and k (see Equation (3)). As the grey dotted line in Figure 6c depicts, the capacitive effect dominates the TPV decay in the low-V_{OC} range, under 750 mV, similar to observations in other solar cell technologies.[31,33,40,41,43] Accounting for the capacitive contribution via Equation (5) and using the differential capacitance data in Figure 4 (grey dotted line), we gain a more direct view of the recombination processes within the CdTe solar cell.

Figure 6c (red star symbols) shows the dependence of effective carrier lifetime τ_{eff} on the bias-light intensity (represented by the V_{OC}), and reveals two distinctive regimes, as expected from Equation (3) and (8) and Figure 1. For V_{OC} values below 850 mV, defect-assisted nonradiative recombination dominates the carrier dynamics with $\tau_{eff} = \tau_{srh} = 580$ ns, which is a constant as it is independent of carrier concentration and so the V_{OC}. This plateau region holds significant importance for the CdTe solar cell community, as being able to quantify the nonradiative recombination lifetime confidently enables researchers and developers to evaluate and refine defect passivation strategies more effectively. It is worth mentioning that in the CdTe community, high surface recombination velocity (v) is often regarded as the main problem limiting the V_{OC}. The nonradiative recombination in the bulk and the surface recombination at the interface are parallel processes, and the shortest of the two will dominate the $\tau_{eff} = 580$ ns

at V_{OC} below 850 mV, according to $\tau_{eff} = \left[\frac{1}{\tau_{rad}} + \frac{1}{\tau_{srh}} + \frac{2v}{d}\right]^{-1}$. This leads to $v = 284\,cm\,s^{-1}$, if surface recombination is the dominant one, which is significantly lower than the values ($v > 1000\,cm\,s^{-1}$) often used in simulation.[5,10,25,27] TPV technique can, therefore, be applied as a diagnostic tool.

As V_{OC} exceeds 850 mV, the radiative recombination process starts to play a role showing a decrease in effective carrier lifetime τ_{eff}. Precise quantification of the radiative recombination requires the stationary carrier density n_{bias} to be known, as indicated in Equation (3) and (8). We achieved n_{bias} utilizing both TPC and TPC data via the differential capacitance method as discussed in a previous section (see Figure 4). Figure 6d presents the effective carrier recombination lifetime across different charge densities. A significant observation is the plateau observed at carrier densities below $1 \times 10^{14}\,cm^{-3}$, indicating a dominance of nonradiative recombination mechanisms in this region, independent of the changes in carrier density. As the charge density surpasses $1 \times 10^{14}\,cm^{-3}$, the effective carrier lifetime transitions to a regime dominated by radiative recombination.

The transition of carrier lifetime from nonradiative to radiative is expected (see Equation (3) and Figure 1) when injection level increases to a point where photogenerated carrier density approaches to or exceeds the doping density $n_{bias} \geq N_A$. The doping density, obtained via *C–V* measurement, is around $1 \times 10^{14}\,cm^{-3}$ for this device (see supporting document). This observation in Figure 6d aligns well with the theoretical model predicting an increased likelihood of radiative recombination as carrier concentration surpasses the doping density, thereby reducing the effective lifetime (see the simulation results and discussion given in the supporting document). Having this charge carrier density data, we are now set to calculate the radiative recombination coefficient *k* using Equation (8). From this analysis, we deduce a radiative recombination coefficient of $\approx 1.1 \times 10^{-9}\,cm^3\,s^{-1}$, aligning well with previous studies that used both steady-state and TRPL measurements on CdTe materials.[37,44]

In comparison to TPV, we conducted TRPL measurements on the device at four different laser fluences. The TRPL data, shown in Figure 6e, revealed distinct features under varying laser fluence. The initial part of the decay ($t < 500$ ns) slowed down with an increase in laser fluence, while the decay's tail accelerated with increased laser fluence. This observation aligns well with the expected drift-diffusion effects dominating early carrier dynamics, resonating with our earlier discussions. The slower initial decay at higher fluences suggests diminished carrier extraction, likely due to charge accumulation-induced electric field alterations at the interface, supporting the findings reported by Kuciauskas et al.[45]

In contrast, the accelerated decay of the TRPL tail with increased laser fluence indicates a rise in the radiative recombination rate with increased carrier concentration, as predicted by Equation (3). Fitting the TRPL data adequately requires a triple-exponential decay model, which still does not capture the entire complexity, particularly at high laser fluence. Thus, we fit the tail of the TRPL decays (Figure 6f), and the extracted lifetime ideally is expected to be consistent for all fluences when it represents the defect-assisted recombination lifetime. The tail lifetime values are indeed closer to the defect-assisted recombination lifetime extracted from TPV. However, it changes from 1009 ns at low fluence to 413 ns at high fluence. This suggests that the tails of the TRPL decays may still be influenced by radiative recombination at higher laser fluences, and/or the tail of the TRPL decay may be affected by charges stored in the electrodes returning to the absorber.[25,27,28] The latter can extend the tail decay constant much longer than the actual defect-assisted lifetime. This means that the capacitance contribution to the TRPL decay should also be accounted for, especially when the TRPL lifetime measured in the completed device is long.

For further evaluation, we also conducted TPV measurements on a low-performing CdTe solar cell, intentionally omitting the front buffer layer (oxygenated CdS) and employing suboptimal Cu doping, to assess their impact on carrier recombination dynamics. These changes indeed resulted in poor device performance with a V_{OC} of 750 mV (supporting document). The TPV results also showed significantly shorter carrier lifetimes (about 100 ns), predominantly governed by defect-assisted recombination, without a clear transition to radiative dominant recombination (supporting document). These findings are consistent with expectations, as both the buffer layer and doping concentration are crucial in influencing carrier recombination rates and, consequently, device performance.

Future studies should focus on exploring the correlation of the nonradiative and radiative recombination dynamics with the various front and back buffer layers, absorber dopants, and the deposition methods, applied in CdTe solar cells, and finding the efficient materials and refining the device fabrication processes to address the device performance limiting factors.[1,6,8,12,46] Such endeavors could lead to significant improvements in solar cell performance, ultimately contributing to the advancement of CdTe photovoltaic technology.

5. Conclusion

In this study, we have demonstrated the application of TPV and TPC techniques in analyzing the recombination dynamics of high-performance cadmium telluride (CdTe) solar cells, overcoming some of the limitations the conventionally used TRPL method has. Our investigation has led to the identification of distinct operational regimes within these cells, where nonradiative and radiative recombination processes dominate based on varying charge carrier densities, aligning well with the theoretical prediction. This distinction is crucial for a thorough understanding of the cell's performance under different operational conditions. A key accomplishment of our research has been the quantification of effective defect-assisted carrier lifetimes and the precise calculation of the radiative recombination coefficient. These metrics are essential for assessing and improving the efficiency of CdTe solar cells. Our findings lay the groundwork for these future efforts, marking a significant step forward in the pursuit of optimizing CdTe solar cells.

6. Experimental Section

CdTe Device Fabrication: CdS window layer of thickness 40 nm was deposited on a fluorine-doped tin oxide (Tech 12D, NSG) substrate under

2% O_2 and 98% Ar gas flow using 2-inch radio-frequency (RF) sputtering. It was followed by an 80 nm CdSe layer deposition using 2-inch RF sputtering under a 1% oxygen and 99% argon flow at room temperature. This step was followed by the deposition of a 3.5 μm CdTe layer through close-space sublimation, conducted at source and substrate temperatures of 660 and 590 °C, respectively, at 1 Torr. Then, the film was treated with wet $CdCl_2$ at 400 °C for 50 min in dry air. Subsequently, 2 mg mL^{-1} CuSCN, dissolved in 30 wt% ammonium hydroxide, was spin-coated at 2000 rpm for 30 s, followed by rapid thermal annealing at 180 °C. The process concluded with the evaporation of a 40 nm Au layer onto the film stack, done through a shadow mask with a cell area of 0.08 cm^2. Further details can be found in our previous publications.[4,6,34]

TPV/TPC Characterization: Measurements were conducted using a custom-built system, which includes a 532 nm excitation laser with a 400 ps pulse width (Market Tech, PowerChip laser PNG-M01550-130) and a high-power white LED (Thorlabs SOLIS-3C) serving as the bias light. Laser intensity was finely adjusted using continuously variable neutral density filters mounted on a translation stage, with computer-controlled adjustments to achieve the desired intensity. Similarly, the intensity of the bias light was regulated directly via computer software. All aspects of data acquisition, including bias-light intensity modulation and data analysis, were managed through a custom-developed Python software suite, utilizing libraries such as NumPy, SciPy, Matplotlib, and Pandas.

Time-Resolved Photoluminescence Measurement (TRPL): The TRPL measurements were conducted using a custom-built setup that includes a Becker & Hickl hybrid photomultiplier tube (HPM100-50) and a Becker & Hickl SPM130 TCSPC module, paired with a Horiba iHR320 monochromator. The excitation source was a Fianium supercontinuum laser, delivering pulses with a 5 ps width at a repetition rate of 250 kHz. These measurements were carried out under standard laboratory air conditions, with the sample being excited at a wavelength of 633 nm. The intensity of the laser was regulated using neutral density filters to ensure precise control over the excitation levels.

Supporting Information

Supporting Information is available from the Wiley Online Library or from the author.

Acknowledgements

This material was based on research sponsored by Air Force Research Laboratory under agreement nos. FA9453-21-C-0056 and FA9453-19-C-1002, as well as the U.S. DOE's Office of Energy Efficiency and Renewable Energy (EERE) under the Solar Energy Technologies Office (SETO), through agreement DE-EE0008974 and through the Alliance for Sustainable Energy, LLC, Managing and Operating Contractor for the National Renewable Energy Laboratory for the U.S. Department of Energy, under award no. 37989. The U.S. Government is authorized to reproduce and distribute reprints for governmental purposes notwithstanding any copyright notation thereon. The views expressed are those of the authors and do not reflect the official guidance or position of the United States Government, the Department of Defense, or of the United States Air Force. The appearance of external hyperlinks does not constitute endorsement by the United States Department of Defense (DoD) of the linked websites or the information, products, or services contained therein. The DoD does not exercise any editorial, security, or other control over the information you may find at these locations. Approved for public release, distribution is unlimited. Public Affairs release approval # AFRL-2023-5466.

Conflict of Interest

The authors declare no conflict of interest.

Data Availability Statement

The data that support the findings of this study are available from the corresponding author upon reasonable request.

Keywords

CdTe solar cells, charge carrier recombinations, defect-assisted carrier lifetimes, radiative recombination coefficients, transient photocurrents, transient photovoltages

Received: February 12, 2024
Revised: March 22, 2024
Published online: April 15, 2024

[1] W. K. Metzger, D. W. Miller, R. Mallick, X. Li, W. Zhang, I. Wang, A. Polizzotti, T. Ablekim, D. H. Cao, D. C. Hamilton, *IEEE J. Photovoltaics* **2022**, *12*, 1435.
[2] M. A. Green, E. D. Dunlop, M. Yoshita, N. Kopidakis, K. Bothe, G. Siefer, X. Hao, *Prog. Photovoltaics: Res. Appl.* **2023**, *31*, 651.
[3] D. Kuciauskas, M. Nardone, A. Bothwell, D. Albin, C. Reich, C. Lee, E. Colegrove, *Adv. Energy Mater.* **2023**, *13*, 2301784.
[4] D. B. Li, S. S. Bista, R. A. Awni, S. Neupane, A. Abudulimu, X. Wang, K. K. Subedi, M. K. Jamarkattel, A. B. Phillips, M. J. Heben, J. D. Poplawsky, D. A. Cullen, R. J. Ellingson, Y. Yan, *Nat. Commun.* **2022**, *13*, 7849.
[5] A. B. Phillips, J. D. Friedl, K. K. Subedi, Z. Song, R. H. Ahangharnejhad, A. Abudulimu, E. Bastola, I. Subedi, M. K. Jamarkattel, Z. Hussain, *Sol. Energy Mater. Sol. Cells* **2024**, *266*, 112689.
[6] A. Abudulimu, D. Li, M. Jamarkatel, Z. Zawisza, S. Wenner, T. Brau, E. Bastola, A. Phillips, M. Heben, Y. Yan, *2023 IEEE 50th Photovoltaic Specialists Conf. (PVSC)*, San Juan, PR, USA, June **2023**, pp. 1–4.
[7] A. Onno, C. Reich, S. Li, A. Danielson, W. Weigand, A. Bothwell, S. Grover, J. Bailey, G. Xiong, D. Kuciauskas, *Nat. Energy* **2022**, *7*, 400.
[8] D. Pokhrel, X. Mathew, K. Khanal Subedi, A. Patel, A. B. Phillips, E. Bastola, A. Abudulimu, M. K. Jamarkattel, S. Rijal, A. Quader, *Sol. RRL* **2022**, *6*, 2200501.
[9] A. Abudulimu, L. Liu, G. Liu, N. Aimaiti, B. Rezek, Q. Chen, *J. Energy Chem.* **2020**, *47*, 132.
[10] A. B. Phillips, J. D. Friedl, Z. Song, R. H. Ahangharnejhad, E. Bastola, Z. H. Rabbani, D.-B. Li, Y. Yan, R. J. Ellingson, M. J. Heben, *2022 IEEE 49th Photovoltaics Specialists Conf. (PVSC)*, Philadelphia, PA, USA, June **2022**, pp. 0701–0701.
[11] M. K. Jamarkattel, A. B. Phillips, D.-B. Li, E. Bastola, G. K. Liyanage, J. D. Friedl, S. S. Bista, D. Pokhrel, A. Quader, P. N. Kaluarachchi, *MRS Adv.* **2022**, *7*, 713.
[12] M. K. Jamarkattel, A. B. Phillips, I. Subedi, A. Abudulimu, E. Bastola, D.-B. Li, X. Mathew, Y. Yan, R. J. Ellingson, N. J. Podraza, *ACS Appl. Energy Mater.* **2022**, *5*, 5484.
[13] A. Abudulimu, J. Kulicek, E. Bastola, A. B. Phillips, A. Patel, D. Pokhrel, M. K. Jamarkattel, M. J. Heben, B. Rezek, R. J. Ellingson, *2022 IEEE 49th Photovoltaics Specialists Conf. (PVSC)*, Philadelphia, PA, USA, June **2022**, pp. 1088–1090.
[14] M. K. Jamarkattel, X. Mathew, A. B. Phillips, E. Bastola, K. K. Subedi, F. K. Alfadhili, A. Abudulimu, J. D. Friedl, R. A. Awni, D.-B. Li, *ACS Appl. Mater. Interfaces* **2022**, *14*, 19644.
[15] A. B. Phillips, J. D. Friedl, P. Ottinger, S. L. Carter, Z. Song, A. Abudulimu, E. Bastola, D.-B. Li, Y. Yan, R. J. Ellingson, *Sol. RRL* **2023**, *7*, 2300545.

[16] R. Sandoval-Torrientes, A. Gavrik, A. Isakova, A. Abudulimu, J. Calbo, J. Aragó, J. Santos, E. Ortí, N. Martín, V. Dyakonov, *J. Mater. Chem. C* **2019**, *7*, 6641.
[17] T. Ablekim, J. N. Duenow, X. Zheng, H. Moutinho, J. Moseley, C. L. Perkins, S. W. Johnston, P. O'Keefe, E. Colegrove, D. S. Albin, *ACS Energy Lett.* **2020**, *5*, 892.
[18] R. Pandey, T. Shimpi, A. Munshi, J. R. Sites, *IEEE J. Photovoltaics* **2020**, *10*, 1918.
[19] J. A. Nelson, *The Physics of Solar Cells*, World Scientific Publishing Company, Singapore **2003**.
[20] A. Abudulimu, K. Eckstein, M. E. Gemayel, I. Namal, A. B. Phillips, R. J. Ellingson, M. J. Heben, T. Hertel, S. B. Meier, L. Lüer, *Sol. RRL* **2022**, *6* 2101010.
[21] A. Sproul, *J. Appl. Phys.* **1994**, *76*, 2851.
[22] T. Kirchartz, J. A. Márquez, M. Stolterfoht, T. Unold, *Adv. Energy Mater.* **2020**, *10*, 1904134.
[23] W. Shockley, W. Read Jr, *Phys. Rev.* **1952**, *87*, 835.
[24] D. Kuciauskas, P. Dippo, A. Kanevce, Z. Zhao, L. Cheng, A. Los, M. Gloeckler, W. K. Metzger, *Appl. Phys. Lett.* **2015**, *107*, 243906.
[25] A. M. Bothwell, C. L. Reich, A. H. Danielson, A. Onno, Z. C. Holman, W. S. Sampath, D. Kuciauskas, *Sol. RRL* **2023**, *7*, 2201029
[26] P. M. Jundt, D. Kuciauskas, J. R. Sites, *IEEE J. Photovoltaics* **2022**, *12*, 501.
[27] J. Moseley, D. Krasikov, C. Lee, D. Kuciauskas, *J. Appl. Phys.* **2021**, *130*, 163105.
[28] L. Krückemeier, B. Krogmeier, Z. Liu, U. Rau, T. Kirchartz, *Adv. Energy Mater.* **2021**, *11*, 2003489.
[29] C. G. Shuttle, B. O'Regan, A. M. Ballantyne, J. Nelson, D. D. C. Bradley, J. de Mello, J. R. Durrant, *Appl. Phys. Lett.* **2008**, *92*, 093311.
[30] D. Kiermasch, L. Gil-Escrig, A. Baumann, H. J. Bolink, V. Dyakonov, K. Tvingstedt, *J. Mater. Chem. A* **2019**, *7*, 14712.
[31] O. J. Sandberg, K. Tvingstedt, P. Meredith, A. Armin, *J. Phys. Chem. C* **2019**, *123*, 14261.
[32] A. Abudulimu, R. Sandoval-Torrientes, I. Zimmermann, J. Santos, M. K. Nazeeruddin, N. Martín, *J. Mater. Chem. A* **2020**, *8*, 1386.
[33] J. Bisquert, *J. Phys. Chem. Lett.* **2022**, *13*, 7320.
[34] D.-B. Li, S. Neupane, S. S. Bista, C. Xiao, A. Abudulimu, M. K. Jamarkattel, A. B. Phillips, M. J. Heben, J. D. Poplawsky, D. A. Cullen, *ACS Energy Lett.* **2023**, *8*, 1529.
[35] W. Becher, Advanced Time-Correlated Single Photon Counting Techniques, Springer, Germany **2005**.
[36] M. M. Taheri, T. M. Truong, S. Li, W. N. Shafarman, B. E. McCandless, J. B. Baxter, *J. Appl. Phys.* **2021**, 130 (16): 163104.
[37] Y. Yuan, G. Yan, C. Dreessen, T. Rudolph, M. Hülsbeck, B. Klingebiel, J. Ye, U. Rau, T. Kirchartz, *Nat. Mater.* **2024**, *23*, 391.
[38] A. Abudulimu, D. Li, L. Chen, J. Santos, I. Zimmermann, N. Katakumbura, T. Brau, E. Bastola, A. Phillips, Z. Song, J. Cabanillas, M. Heben, M. K. Nazeeruddin, N. Martin, Y. Yan, R. Ellingson, *2023 IEEE 50th Photovoltaic Specialists Conf. (PVSC), San Juan, PR, USA*, June **2023**, pp. 1–5.
[39] Z. S. Wang, F. Ebadi, B. Carlsen, W. C. H. Choy, W. Tress, *Small Methods* **2020**, *4*, 2000290.
[40] D. Kiermasch, A. Baumann, M. Fischer, V. Dyakonov, K. Tvingstedt, *Energy Environ. Sci.* **2018**, *11*, 629.
[41] R. A. Street, *Phys. Rev. B* **2011**, *84*, 075208.
[42] L. Castaner, E. Vilamajo, J. Llaberia, J. Garrido, *J. Phys. D Appl. Phys.* **1981**, *14*, 1867.
[43] S. Li, R. Nishikubo, T. Wada, T. Umeyama, H. Imahori, A. Saeki, *Polym. J.* **2022**.
[44] P. Ščajev, S. Miasojedovas, A. Mekys, D. Kuciauskas, K. G. Lynn, S. K. Swain, K. Jarašiūnas, *J. Appl. Phys.* **2018**, *123*, 025704.
[45] D. Kuciauskas, C. L. Perkins, M. Nardone, C. Lee, R. Mallick, G. Xiong, *Sol. RRL* **2023**, *7*, 2300073.
[46] M. K. Jamarkattel, A. B. Phillips, I. Subedi, A. Abudulimu, E. Bastola, D.-B. Li, Z. Song, X. Matthew, Y. Yan, R. J. Ellingson, *2022 IEEE 49th Photovoltaics Specialists Conf. (PVSC)*, Philadelphia, PA, June **2022**, pp. 0972–0974.